Journal of Computational Neuroscience 15, 283–298, 2003

Analysis of State-Dependent Transitions in Frequency and Long-Distance Coordination in a Model Oscillatory Cortical Circuit

DAVID J. PINTO
Department of Neuroscience, Brown University, Box 1953, Providence, RI 02912, USA
dpinto@bu.edu

STEPHANIE R. JONES
Harvard Medical School, NMR Center, Massachusetts General Hospital, Charlestown, MA 02129, USA

TASSO J. KAPER AND NANCY KOPELL
Department of Mathematics and Center for Biodynamics, Boston University, Boston, MA 02215, USA

Abstract. Changes in behavioral state are typically accompanied by changes in the frequency and spatial coordination of rhythmic activity in the neocortex. In this article, we analyze the effects of neuromodulation on ionic conductances in an oscillating cortical circuit model. The model consists of synaptically-coupled excitatory and inhibitory neurons and supports rhythmic activity in the alpha, beta, and gamma ranges. We find that the effects of neuromodulation on ionic conductances are, by themselves, sufficient to induce transitions between synchronous gamma and beta rhythms and asynchronous alpha rhythms. Moreover, these changes are consistent with changes in behavioral state, with the rhythm transitioning from the slower alpha to the faster gamma and beta as arousal increases. We also observe that it is the same set of underlying intrinsic and network mechanisms that appear to be simultaneously responsible for both the observed transitions between the rhythm types and between their synchronization properties. Spike time response curves (STRCs) are used to study the relationship between the transitions in rhythm and the underlying biophysics.

Keywords: rhythms, synchrony, neocortex, neuromodulation, alpha, beta, gamma, arousal

1. Introduction

Behavioral states are accompanied by rhythmic neocortical activity characterized by approximate frequency ranges and by the locations in the brain where the rhythms appear. Rhythms in the gamma frequency range (30–80 Hz) are observed during alert and attentive behaviors, and in response to visual processing in human EEGs (Keil et al., 2001; Tallon-Baudry et al., 1999). Beta rhythms (12–30 Hz) are observed during sensory processing (Marrufo et al., 2001; Muller, 2000), immediately following sensory evoked gamma (Haenschel et al., 2000; Pantev, 1995) and in sensory-motor coordination (Farmer, 1998). Alpha rhythms (7–14 Hz) are observed during periods of unfocused or resting behavior (Roelfsema et al., 1997; Nunez et al., 2001) and rhythms with a similar frequency range, known as mu, are found in preparation for exploratory movements (Fanselow and Nicolelis, 1999). Evidence suggests that sensory evoked beta rhythms synchronize over longer spatial distances than do gamma rhythms (von Stein and Sarnthein, 2000; von Stein et al., 1999), and that alpha rhythms need not synchronize over cortical distance (Roelfsema et al., 1997). In this paper, we

are concerned with the transitions among gamma, beta, and alpha rhythms, and how the long-distance synchronization properties of networks displaying these rhythms change with each transition.

Each of the rhythms can be associated with different sets of intrinsic conductances. Gamma rhythms can be formed from interactions between excitatory (E) cells and inhibitory (I) cells, and require no currents other than those involved in spike generation along with $GABA_A$ and *AMPA* mediated synaptic interactions (Whittington et al., 2000; Traub et al., 1999). A minimal network that can generate gamma rhythms requires only reciprocal connections (i.e., E to I and I to E); neither recurrent excitatory (E to E) nor inhibitory (I to I) connections are needed (unlike "interneuron gamma"; for details, see Whittington et al., 1995).

In vitro studies suggest that beta rhythms in hippocampal slices involve ionic conductances in addition to those required by gamma. Tetanic stimulation of hippocampal slices induces rhythmic gamma activity that spontaneously changes to beta frequencies among pyramidal neurons; the interneuron network continues to oscillate at gamma (Traub et al., 1999; Whittington et al., 1997; for discussion, see Kopell et al., 2000). The transition involves the re-emergence of a slow afterhyperpolarizing potassium current (AHP) that is suppressed by the initial tetanic stimulus. The transition also involves the potentiation of excitatory synapses that occurs as a consequence of synchronous activity during the gamma rhythm (Whittington et al., 1997). Both gamma and beta rhythms are tightly coupled to $GABA_A$ inhibition and disappear in the presence of $GABA_A$ blockers (Whittington et al., 2000). Spontaneous gamma to beta transitions have been observed both *in vitro* (Traub et al., 1999; Whittington et al., 1997) as well as *in vivo* (Haenschel et al., 2000).

Alpha rhythms are found in many regions of the brain and may be generated by a number of potentially different mechanisms. In the thalamus, alpha rhythms are believed to involve the hyperpolarization-activated *h*-current and the hyperpolarization-deinactivated T-current (Sherman, 2001; Destexhe et al., 1993). This biophysical mechanism may play a role in the generation of cortical alpha rhythms as well. Some neurons of cortical layer V, from which cortical alpha is believed to originate (Silva et al., 1991; da Silva, 1991; Kristiansen and Courtois, 1949), also exhibit hyperpolarization activated inward currents (Timofeev et al., 2002; Pare and Lang, 1998; Connors and Amitai, 1997; de la Pena and Geijo-Barrientos, 1996). Moreover, experimental data obtained from intact cortex (Steriade et al., 1998; Castro-Alamancos and Connors, 1996a), from isolated cortical slabs (Timofeev et al., 2002), and from cortical slices (Castro-Alamancos and Connors, 1996b) demonstrate that rhythmic stimulation of cortical neurons at frequencies corresponding to alpha result in augmented synaptic responses that are likely to be originating from cortical layer V (Castro-Alamancos and Connors, 1996a, b). Based on this mechanism, Jones et al. (2001) developed and analyzed a model for cortical alpha; related thalamic models include those by Wang et al. (1995) and Destexhe et al. (1996). Analyses of these models suggest that, in contrast to both gamma and beta, the frequency of the alpha rhythm is dominated by the time course of the h- and T-currents and is less strongly affected by the time course of synaptic inhibition.

Gamma, beta, and alpha rhythms also have different properties with respect to long-distance synchronization. Previous studies have examined a mechanism for synchronization that involves a firing pattern of interneurons known as "doublets"; the interneurons fire twice each cycle, once after excitation from local pyramidal cells, and once in response to excitation from distant pyramidal cells. Doublets have been observed both in detailed biophysical models and in slice preparations (Traub et al., 1996). For gamma rhythms, minimal models have reproduced and explained the role of doublets in creating a synchronizing feedback loop and have explored the parameter regimes in which such a mechanism can work (Ermentrout and Kopell, 1998). For beta rhythms, the additional AHP current extends the range of conduction delays over which inhibitory doublets can synchronize activity (Kopell et al., 2000). For alpha rhythms, inhibition-activated inward currents effectively reverse the role of inhibition in spike timing, so that inhibitory doublets act to destabilize synchrony over distance (Jones et al., 2001). A generalization of the synchronizing role of inhibitory doublets in the context of spatially extended networks with a range of conduction delays is presented in Karbowski and Kopell (2000) (for related work see Bibbig et al., 2001).

Transitions between cortical rhythms, and the corresponding transitions in behavioral state, may reflect changes in the level of neuromodulation acting on cortical circuits. It has long been known, for instance, that endogenous levels of cortical acetylcholene (ACh) increase during periods of wakefulness and/or sensory stimulation (Celesia and Jasper, 1966; for review, see Detari et al., 1999). Lesions to the basal forebrain, a

major source of cholinergic innervation to cortex, result in decreased levels of both endogenous ACh and high frequency (e.g., gamma) activity (Buzsaki et al., 1988; Lo Conte et al., 1982). Conversely, basal forebrain activation, either chemically or electrically, results in increased levels of ACh in cortex, increased wakefulness, and increased gamma frequency activity (Cape and Jones, 1998; Dringenberg and Vanderwolf, 1997; for other references, see Cape and Jones, 2000).

In this paper, we use a model cortical circuit to investigate possible biophysical mechanisms underlying state-dependent transitions in the frequency of cortical rhythms and in their ability to synchronize over distance. We analyze the biophysical model using a low-dimensional map that describes the difference in firing times between spatially separated oscillating circuits from cycle to cycle, as described previously by Jones et al. (2000) and Kopell et al. (2000). The shape of the map depends on the intrinsic and synaptic currents expressed during a particular rhythmic state and predicts directly whether the synchronous state is stable or unstable. Changes in behavioral state are modeled according to known effects of ACh on cortical neurons, including those of cortical layer V (Detari et al., 1999; Hasselmo, 1995; McCormick, 1992). We incorporate these changes by systematically varying the resting depolarization level of individual neurons and the maximal conductance of the AHP current.

Our analysis has three primary goals. First, we demonstrate that the effects of neuromodulation on ionic conductances are sufficient to induce a transition from the slower alpha rhythm to the faster gamma and beta rhythms, consistent with behavioral changes. Second, we examine how these biophysical changes affect the maps associated with synchrony over cortical distances. Third, we use the maps to explain the mechanisms by which neuromodulation affects changes in synchrony.

We find that a single neuronal circuit can support rhythmic activity in either the gamma, beta, or alpha frequency ranges under different states of arousal; the rhythm changes from alpha to gamma/beta as arousal increases. Transitions in frequency are accompanied by corresponding transitions in synchrony over cortical distance; gamma and beta rhythms synchronize over distance, alpha rhythms do not. Analysis of the low-dimensional maps suggests that the same set of underlying intrinsic and network mechanisms within the circuit appear to be simultaneously responsible for both the observed transitions between the rhythm types and between their synchronization properties. Taken together, our results provide an explanation for how neuronal dynamics within a single cortical circuit can be transformed by neuromodulation from a system that generates spatially synchronous gamma and beta rhythms into one that generates spatially asynchronous alpha rhythms.

2. Methods

In this section, we describe our cortical circuit model and the equations governing its function. We also briefly review the use of spike time response curves (STRCs) for analyzing synchrony in coupled oscillators. The methods are similar to those used in previous studies (Acker et al., 2002; Jones et al., 2000; Kopell et al., 2000; Ermentrout and Kopell, 1998).

2.1. *Biophysical Model*

Each cortical oscillator consists of two synaptically coupled neurons, one excitatory and one inhibitory. Both are modeled by current balance equations describing the membrane voltage,

$$\begin{aligned} C\frac{dV_E}{dt} &= I_L + I_{\mathrm{Na}} + I_{\mathrm{K}} + I_T + I_h + I_{\mathrm{AHP}} \\ &\quad + I_{\mathrm{APP}_e} + I_{\mathrm{GABA}_A} \\ C\frac{dV_I}{dt} &= I_L + I_{\mathrm{Na}} + I_{\mathrm{K}} + I_{\mathrm{APP}_i} + I_{\mathrm{AMPA}} \\ I_{\mathrm{ion}}(V) &= g_{\mathrm{ion}} a^p b^q (E_{\mathrm{ion}} - V), \end{aligned}$$

where $C = 1\,(\mu\mathrm{F/cm}^2)$ is the membrane capacitance, $V_j\,(\mathrm{mV})$ is the membrane potential of cell j, I_{ion} are ionic currents detailed below, g_{ion} is the maximal conductance for the given ionic channel, a and b are the proportion of channels that are activated and deinactivated, respectively, p and q are integers, and E_{ion} is the reversal potential for the given ion.

The passive leak current is $I_L(V) = g_L(E_L - V)$, where $g_L = 0.1\,(\mathrm{mS/cm}^2)$ and $E_L = -67\,(\mathrm{mV})$. The fast sodium current is $I_{\mathrm{Na}}(V) = g_{\mathrm{Na}} m^3 h(E_{\mathrm{Na}} - V)$ and the delayed rectifier potassium current is $I_{\mathrm{K}}(V) = g_{\mathrm{K}} n^4(E_k - V)$, where $g_{\mathrm{Na}} = 100$, $g_{\mathrm{K}} = 80$, $E_{\mathrm{Na}} = 50$, and $E_{\mathrm{K}} = -100$. The kinetic equations for the activation and deinactivation variables, m, h, and n, take the form $da/dt = \alpha_a(1 - a) - \beta_a a$, where $\alpha_m = 0.32(V + 54)/(1 - \exp(-(V +$

54)/4)), $\beta_m(V) = -0.28(V+27)/(\exp((V+27)/5) - 1)$, $\alpha_h(V) = 0.128\exp(-(50+V)/18)$, $\beta_h(V) = 4/(1+\exp(-(V+27)/5))$, $\alpha_n(V) = 0.032(V+52)/(1-\exp(-(V+52)/5))$, $\beta_n(V) = 0.5\exp(-(57+V)/40)$. The afterhyperpolarization potassium current is $I_{\mathrm{AHP}}(V) = g_{\mathrm{AHP}} w(E_{\mathrm{K}} - V)$, where g_{AHP} is varied as a function of arousal as described below. Results are similar using any AHP current with an appropriate decay time. The hyperpolarization activated low threshold calcium current is $I_T(V) = g_T m_T^2 h_T(E_{\mathrm{Ca}} - V)$ and mixed cation current is $I_h(V) = g_h r(E_h - V)$, where $g_T = 2.7$, $g_h = 0.25$, $E_{\mathrm{Ca}} = 125$, $E_h = -43$. The kinetic equations for w, m_T, h_T, and r take the form $da/dt = (a_\infty - a)/\tau_a$, where $w_\infty(V) = 1/(1+\exp(-(V+35)/10))$, $\tau_w(V) = 400/(3.3\exp((V+35)/20) + \exp(-(V+35)/20))$, $\tau_{m_T}(V) = .44 + .15/(\exp((V+27)/10) + \exp(-(V+102)/15))$, $h_{T,\infty}(V) = 1/(1+\exp((V+80)/5))$, $\tau_{h_T}(V) = 22.7 + .27/(\exp((V+48)/4) + \exp(-(V+407)/50))$, $r_\infty(V) = 1/(1+\exp((V+75)/5.5))$, $\tau_r(V) = 1/(\exp(-14.59 - .086 * V) + \exp(-1.87 + .0701 * V))$. The currents I_{APP_e} and I_{APP_i} are applied directly and varied as a function of arousal as described below. All currents are expressed in units of $\mu\mathrm{A/cm}^2$. The kinetic equations and parameter values for intrinsic currents were taken from previous modeling studies (Kopell and Ermentrout, 2000; Jones et al., 2000; Destexhe et al., 1996; Wang et al., 1995), and were chosen to qualitatively reproduce the intrinsic firing properties of individual cortical neurons.

The synaptic currents are $I_{\mathrm{AMPA}}(V) = g_{ei}\ AMPA\ (E_{\mathrm{AMPA}} - V)$ and $I_{\mathrm{GABA}_A}(V) = g_{ie}\ GABA_A\ (E_{\mathrm{GABA}_A} - V)$, where $E_{\mathrm{AMPA}} = 0$, $E_{\mathrm{GABA}_A} = -80$, $g_{ei} = 0.2$, and $g_{ie} = 1.0$. The kinetic equations for the synaptic conductances $AMPA$ and $GABA_A$ take the form $da/dt = k_a(V)(1-a) - a/\tau_a$, where $k_{\mathrm{AMPA}}(V_e) = 5 * (1 + \tanh(V_e)/4)$, $\tau_{\mathrm{AMPA}} = 2$ (ms), $k_{\mathrm{GABA}_A}(V_i) = 2 * (1 + \tanh(V_i)/4)$, and $\tau_{\mathrm{GABA}_A} = 10$. In two cell cortical oscillators, only reciprocal synaptic connections are included (i.e., g_{ei} and g_{ie}). Four cell cortical oscillators described below include both reciprocal and recurrent connections (i.e., g_{ee} and g_{ii}), but individual neurons do not synapse onto themselves (i.e., no autaptic connections). Inclusion of autaptic connections yields results qualitatively the same as those presented so long as connection strengths are normalized to reflect the increased number of synapses (data not shown; for details, see Jones et al., 2000). The kinetic equations for synaptic currents were taken from previously published modeling studies (Destexhe et al., 1998). The relative strengths of inhibitory and excitatory synapses are modeled using lumped parameters that yield behaviors similar to what is seen in real circuits and are similar to those used in previous studies (Jones et al., 2000; Kopell et al., 2000; Ermentrout and Kopell, 1998).

To investigate the ability of oscillating circuits to synchronize over spatially separated cortical regions, we synaptically coupled two cortical oscillators. The physical separation between oscillators is modeled using a time delay, $\delta > 0$, with longer delays corresponding to greater distances. Only distant excitatory (AMPA) synapses are considered. However, both the excitatory and inhibitory neuron of an oscillator receive distant excitatory input. (Distant inhibitory synapses also exist in neocortex, but are notably more sparse (Kisvarday et al., 1994).) Synaptic connection strengths were chosen to reflect previous anatomical and functional studies of connectivity in neocortex. For instance, synapses between distant neurons are weaker than those between local neurons ($g_{ei} = 0.2$ for local synapses and $g_{ee} = g_{ei} = .1$ for distant synapses), reflecting a decreasing density of synaptic connections over distance (e.g., Lund et al., 1993). All results are qualitatively the same, however, so long as the strengths of both local and distant excitatory synapses are such that a spike in either excitatory neuron evokes a single spike in the local inhibitory neuron, with the net result being that one observes spike doublets in the inhibitory neuron (data not shown).

An increase in arousal is represented by an increase in the level of the neuromodulator ACh. In turn, the effects of ACh are modeled according to some of its known effects on cortical neurons, i.e., as ACh increases, the maximal conductance (g_{AHP}) of the afterhyperpolarization potassium current decreases and the resting potential increases in individual neurons (Hasselmo, 1995; McCormick, 1992). The latter is most likely due to the effect of ACh on the leak conductance (Hasselmo, 1985; McCormick, 1992). However, to be consistent with previous studies, we instead vary the tonic level of applied current. Changing the leak conductance leads to results identical to those presented (data not shown).

In hippocampal slices, the transition from gamma to beta rhythms is characterized by the re-emergence of an AHP-current and by the potentiation of excitatory synapses onto excitatory neurons (Whittington et al., 1997). Previous analysis has demonstrated that strong excitatory synapses are not required for, but also do

not impede, the generation and/or synchronization of gamma rhythms (Kopell et al., 2000; Traub et al., 1999). In detailed models, very strong excitatory synapses lead to bursting behavior (Traub et al., 1999) and can be disruptive of two-site synchrony (Fuchs et al., 2000). Thus, to simplify the analysis, excitatory synaptic strengths were fixed at sufficient levels for the generation of beta rhythms when AHP-currents are active, but below levels that lead to bursting or uncontrolled activity.

2.2. *Spike Time Response Curves*

2.2.1. Analysis. In this section, we briefly review the role of spike time response curves (STRCs) in the analysis of synchrony. STRCs are similar to phase response curves, but provide response measures in terms of time rather than phase (Kopell and Ermentrout, 2001; Jones et al., 2000; Winfree, 1980; for discussion, see Acker et al., 2002).

Figure 1 presents a schematic of two identical cortical oscillators coupled with a delay of δ; connections crossing the dashed line are delayed. Both oscillators consist of an excitatory and inhibitory neuron, denoted as E_1, I_1 and E_2, I_2. Following Ermentrout and Kopell (1998), let

$$\begin{aligned} t_1 &= \text{time when } E_1 \text{ fires} \\ t_2 &= \text{time when } E_2 \text{ fires} \\ \overline{t_1} &= \text{next time when } E_1 \text{ fires} \\ \overline{t_2} &= \text{next time when } E_2 \text{ fires.} \end{aligned}$$

After E_2 fires, it takes an amount of time equal to $t_1 + \delta - t_2$ for the oscillator containing E_2 to receive excitatory input from E_1. Thus

$$\overline{t_2} = t_2 + STRC(t_1 + \delta - t_2),$$

where $STRC(t)$ is a function that describes the advance or delay of the firing of an excitatory neuron for a given arrival time of excitatory input onto the oscillator containing that neuron. Note that, if E_2 has an intrinsic firing period of T_2, then $STRC(t) \equiv 0$ for $t > T_2$. That is, if input from E_1 arrives after time T_2, then the period of E_2 during the present cycle is unaffected.

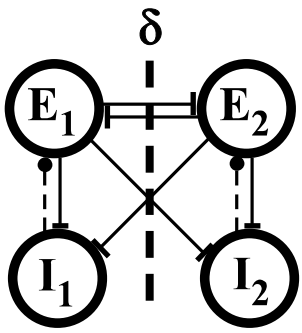

Figure 1. Schematic of circuit model. The figure presents a schematic of two identical cortical oscillators synaptically coupled with a delay of δ ms. Each oscillator consists of a single excitatory and inhibitory neuron (E_1, I_1 and E_2, I_2). Solid and thin dashed lines denote excitatory and inhibitory synaptic connections, respectively. Connections crossing the thick dashed line are delayed by δ ms.

Define $\Delta = t_2 - t_1$ as the difference in spike times between E_2 and E_1. Similarly, $\bar{\Delta} = \overline{t_2} - \overline{t_1}$. The synchronized state corresponds to $\bar{\Delta} = \Delta = 0$. From the above definitions, we construct a 1-D map, H_δ, for each fixed δ, that describes the difference in spike time in the next cycle, $\bar{\Delta}$, in terms of the difference in spike term in the previous cycle, Δ, i.e.,

$$\begin{aligned} \bar{\Delta} &= t_2 - t_1 + STRC(t_1 + \delta - t_2) - STRC(t_2 + \delta - t_1) \\ &= \Delta + STRC(-\Delta + \delta) - STRC(\Delta + \delta) \\ &\equiv H_\delta(\Delta). \end{aligned}$$

Note that since $H_\delta(0) = 0$, the synchronous solution exists as a fixed point of the map.

To evaluate the stability of synchrony, we consider $H'_\delta(\Delta)$ at $\Delta = 0$, where the prime denotes the derivative with respect to Δ. From the definition of H_δ, we find

$$\begin{aligned} H'_\delta(\Delta) &= 1 - STRC'(-\Delta + \delta) - STRC'(\Delta + \delta) \\ H'_\delta(0) &= 1 - 2STRC'(\delta). \end{aligned}$$

The fixed point $\Delta = 0$ is stable when $|H'_\delta(0)| < 1$ (Devaney, 1992) or, equivalently, when

$$0 < STRC'(\delta) < 1.$$

This mathematical condition describes a straightforward relationship between the stability of synchrony and the shape of the STRC. Using our model, we generate STRCs numerically and consider their slope at different delays to predict when two oscillators will or will not synchronize.

The general hypotheses underlying the use of STRC analysis are that (1) the effect of a given perturbation depends only on the time that it is received within a given cycle and (2) oscillators approximately return to their periodic waveform within one cycle after an external perturbation. In the present model, the validity of the first assumption is supported by the fact that each

perturbation is caused by a short (relative to the oscillator period) EPSC having a stereotyped temporal profile. STRCs obtained using different synaptic strengths (within the ranges described above) were qualitatively similar to those presented below (data not shown). The validity of the second assumption is supported by the fact that the voltage spike marking the end of each cycle effectively resets all of the voltage gated channels to nearly fixed values. In the case of the slow AHP current, increasing the AHP conductance results in longer cycle periods, allowing more time for the current to decay before the start of the next cycle; indeed, the AHP conductance, when sufficiently large, effectively determines the period. Finally, to justify directly the use of STRC analysis for understanding the mechanisms underlying synchrony, we confirm that the analytic results derived from the STRCs match those derived from numerical simulations using the full model.

2.2.2. Numerics. All simulations were performed using the XPP software package (GB Ermentrout, available at www.pitt.edu/∼phase). Equations were integrated using a fourth order Runge-Kutta method with a 20 μs time step. The STRC construction process consists of taking a single cortical oscillator (one excitatory and one inhibitory neuron), imposing specifically timed excitatory synaptic inputs onto both neurons, and measuring the subsequent firing period of the excitatory neuron (cf. Fig. 4). STRCs were constructed numerically from XPP output files using PERL scripts specifically written for the task (ActivePerl 5.6, ActiveState Software). The stability of synchronous solutions was tested numerically by integrating the equations for a coupled pair of oscillators with each starting from slightly different initial conditions. A number of different initial conditions were examined for each simulation. Plots and figures were constructed using the Origin 5.0 (Microcal Software) and Canvas 8.0 (Deneba Software) software packages.

2.3. Definitions of Rhythmic Activity

Our working definitions of gamma, beta, and alpha rhythms classify each in terms of firing pattern and/or the activation of intrinsic currents. Since firing patterns can change when two local circuits are coupled, we will use the patterns of the coupled system for our classification. As described below, our definition of each rhythm refines the standard descriptions usually stated in terms of activity frequency.

We first review the classification of gamma and beta for the *in vitro* hippocampal preparation on which our classification is based (Traub et al., 1999; Whittington et al., 1997). In that preparation, both E and I neurons fire on every cycle during gamma. During beta, I neurons fire at gamma frequencies while E neurons fire on every other I neuron cycle. Since the E neurons skip the same cycles, the population firing rate reflects their lower firing rate. Note that, unlike gamma, this form of beta involves intrinsic (i.e., non-synaptically evoked) spikes from the interneurons (for review, see Whittington et al., 2000).

When two circuits are synaptically coupled (within a range of coupling strengths), I neurons fire an extra spike on each cycle evoked by excitation coming from the distant circuit (i.e., "doublets"). In the model, rhythmic activity in a coupled pair of oscillators is classified as gamma if the inhibitory neurons produce only spike doublets on each cycle and the level of h-current activation on each cycle remains below some threshold (see below). Rhythms are classified as beta if the inhibitory neurons produce spike doublets *plus* one intrinsic (i.e., non-synaptically evoked) spike on each cycle.

Our definition of alpha involves the use of h-current activation; rhythms are classified as alpha if inhibitory neurons produce only spike doublets on each cycle *and* the h-current activation in the excitatory neuron (i.e., r in the equation for I_h) reaches some threshold value on every cycle. Note that the firing pattern of alpha is the same as gamma. The choice of h-current activation threshold is somewhat arbitrary; it corresponds to the value at which the role of inhibitory spike doublets changes from stabilizing to destabilizing synchrony (as shown below in Fig. 3). For the results described below, the threshold was set at $r = .09$. However, for all network parameters we examined, an h-current activation threshold value corresponding to the transition from synchrony to asynchrony could always be determined.

Figure 2b–d present voltage traces from the excitatory (thick black traces) and inhibitory neuron (thin gray traces) of one of the oscillators during each rhythmic state. Figure 2a shows the range of frequencies observed. Note that the frequencies of beta rhythms overlap those of both gamma and alpha, and gamma rhythms emerge at frequencies usually associated with the slower alpha rhythm. However, beta can be readily distinguished from the other rhythms in terms of its firing pattern; only beta rhythms involve intrinsic (i.e., non-synaptically evoked) spikes from the inhibitory neuron. Moreover, we argue in the discussion that the

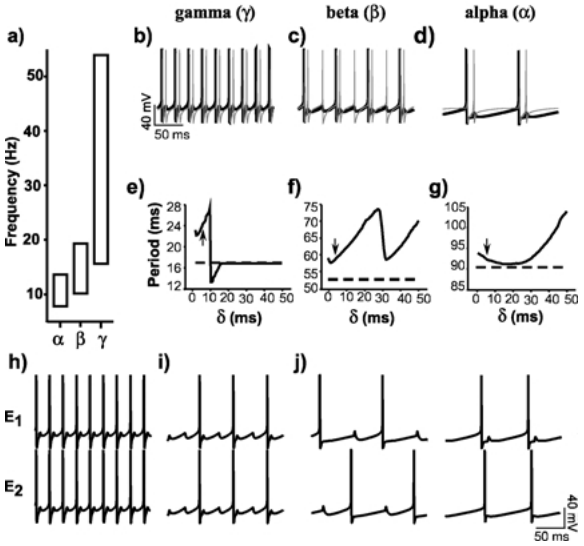

Figure 2. Alpha, beta, and gamma rhythms emerge from the same coupled pair of cortical oscillators. Panel (a) presents the range of firing frequencies exhibited by the excitatory neurons during gamma, beta and alpha rhythms. Panels (b)–(d) present example firing patterns of the excitatory (dark trace) and inhibitory (light trace) neuron from one of the oscillators during gamma, beta, and alpha rhythms, respectively. Panels (e)–(g) present STRCs generated from one of the cortical oscillators under conditions that lead to gamma, beta, and alpha rhythms, respectively. The dashed line indicates the intrinsic period of the excitatory neurons. The small arrows mark the STRC at the point $\delta = 5$ ms; the STRC slope at $\delta = 5$ ms is negative during alpha, and positive during both gamma and beta. Panels (h)–(j) present voltage traces from the two excitatory neurons during gamma, beta, and alpha rhythms, respectively. Two examples of alpha rhythms are presented. Parameter values for applied currents and g_{AHP} are as indicated by the three boxed values in Fig. 3a below (gamma, $g_{\mathrm{AHP}} = 0.0$, $I_{\mathrm{APP}_e} = 4.5$,$I_{\mathrm{APP}_i} = 1.1$; beta, $g_{\mathrm{AHP}} = 1.0$, $I_{\mathrm{APP}_e} = 4.0$,$I_{\mathrm{APP}_i} = 1.0$; alpha, $g_{\mathrm{AHP}} = 1.0$, $I_{\mathrm{APP}_e} = -0.25$, $I_{\mathrm{APP}_i} = -0.1$).

"slow gamma" rhythm is an artifact of the small and non-noisy networks we are using, and we ignore it in the analysis that follows.

3. Results

3.1. STRCs Predict Synchrony

As parameters mimicking states of arousal are varied (as described below), alpha (α), beta (β), and gamma (γ) rhythms emerge from the same synaptically coupled pair of cortical oscillators (Fig. 2b–d). Figure 2e–g present STRCs, obtained as described in Methods, from one of the cortical oscillators under the same three conditions as used to obtain Fig. 2b–d. The horizontal axis represents the delay at which imposed input is received. The vertical axis represents the subsequent firing period of the excitatory neuron. The dashed line indicates the firing period of the excitatory neuron when no input is imposed. Note that nearly all extrinsic perturbations result in longer firing periods.

As described in Methods, the slope of the STRC at each delay predicts whether or not a pair of synaptically coupled oscillators will synchronize. With a coupling delay of 5 ms, for instance (Fig. 2e–g, arrows), the slope of the STRC is between zero and one under conditions that induce gamma or beta, and negative for alpha. This suggests that a pair of oscillators coupled with a 5 ms delay will synchronize under conditions that induce gamma or beta, but not alpha. The predictions are confirmed in Fig. 2h–j, which present voltage traces of the two excitatory neurons from a coupled pair of oscillators during each rhythmic state. The traces are perfectly synchronized for both gamma and beta rhythms (Fig. 2h and i), while the alpha rhythm exhibits asynchrony (Fig. 2j). Two examples of asynchronous alpha are presented to indicate that a number of asynchronous solutions may exist.

More generally, for all of the parameter sets that we examined, values that yield STRCs having slope between zero and one (respectively negative) lead to synchronous (respectively asynchronous) activity in the full network. This provides the necessary justification for our use of the low-dimensional maps to understand the mechanisms underlying synchrony in our model oscillatory cortical circuit.

3.2. Transitions Between Rhythms

Transitions between alert or attentive states and unfocused or rest states are accompanied by changes in rhythmic activity and in levels of neuromodulation. We model changes in arousal by altering two key parameters, (1) the level of tonic drive to both excitatory and inhibitory neurons and (2) the maximal AHP conductance in the excitatory neuron.

Figure 3 presents frequency matrices showing the dependence on these two parameters of rhythmic activity exhibited by a coupled pair of oscillators and their ability to synchronize over distance. The coupling delays are 5 ms and 15 ms, respectively, in Fig. 3a and b. Matrices generated at other delays are similar (3–25 ms; data not shown). Each matrix presents the firing frequency averaged from the two excitatory

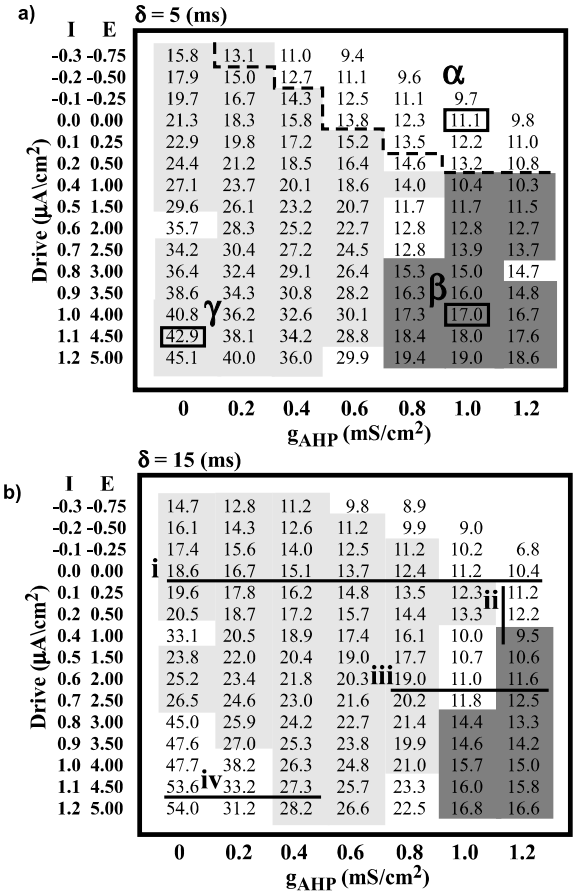

Figure 3. Frequency and synchrony change with parameters of arousal. Panels (a) and (b) present frequency matrices showing the averaged frequency of the two excitatory neurons from a coupled pair of cortical oscillators for a given value of g_{AHP} (x-axis) and tonic drive to each cell type (y-axis). The coupling delay (δ) is 5 ms in panel (a) and 15 ms in panel (b). The two y-axis scales indicate the current applied to the excitatory (E) and inhibitory (I) neurons, respectively. Shaded frequency values indicate parameter states in which the excitatory neurons are synchronous; light shaded states indicate synchronous gamma or alpha rhythms, dark shaded states indicate beta. The dashed line in panel (a) indicates the lower boundary of states that exhibit alpha rhythms. The three boxed values in panel (a) indicate states used to generate data presented in Fig. 2 above and in Figs. 4 and 5 below. The four lines in panel (b) indicate state transitions examined in Fig. 6 below.

neurons for a given value of g_{AHP} (horizontal axis) and tonic drive to each cell type (vertical axis). Shaded backgrounds indicate parameter states in which the two excitatory neurons are precisely synchronized (i.e., less than 1 ms difference in spike time). As predicted by the STRCs in Fig. 2, nearly all of the gamma and beta states are synchronous with a coupling delay of 5 ms, indicated by the light and dark shadings, respectively. States exhibiting alpha rhythms as defined above ($r \geq .09$) are bounded below by the dashed line in Fig. 3a; the boundary in Fig. 3b is approximately the same. In contrast with gamma and beta, nearly all of the alpha states are asynchronous with a coupling delay of 5 ms. The three boxed numbers in Fig. 3a indicate parameter values used to generate voltage traces and STRCs presented in Fig. 2 (above) and Figs. 4 and 5 (below). The four lines labeled i–iv in Fig. 3b indicate the transitions in rhythm and synchrony examined in detail in Fig. 6 (below) using STRC analysis.

The frequency matrices also show the synchronization properties of each type of rhythm over cortical distance. For instance, parameter states near the alpha rhythm boundary (i.e., dashed line in Fig. 3a) lead to rhythms that are asynchronous over short delays (5 ms, Fig. 3a) but synchronous over long delays (15 ms, Fig. 3b). By contrast, high frequency gamma rhythms (lower left corner) are synchronous over short delays but asynchronous over long delays. Beta is synchronous for delays of both 5 and 15 ms.

Frequency matrices have also been obtained using different levels of tonic drive to the inhibitory (I) versus excitatory (E) neuron (y-axis), with similar results. For instance, increasing drive to the I cells relative to the E cells shifts the boundary between gamma and beta upward and to the left. Intuitively, this is because additional tonic drive to the inhibitory neurons results in higher firing rates, enabling the intrinsic (non-evoked) inhibitory spike to emerge even when excitatory neurons are also firing rapidly (i.e., when the AHP conductance is weak).

The matrices can be used to conceptualize the relationship between state-transitions and the underlying biophysics. For instance suppose that, beginning from an alpha state of quiet wakefulness (for example, upper right boxed state in Fig. 3a), a subject is required to perform a task. When the task begins, the subject becomes aroused. ACh enters the cortex from the basal forebrain (Cape and Jones, 1998), blocking both AHP currents and passive leak channels (Hasselmo, 1995; McCormick, 1992). As a result, activity shifts from alpha to gamma (e.g., the lower left boxed state). As the AHP current recovers, excitatory neurons fire more slowly, and activity shifts to beta (Haenschel et al., 2000) (e.g., the lower right boxed state). Finally, when the task is complete, the subject returns to a quiet state, ACH levels drop, the neurons become less depolarized (Detari et al., 1999), and activity returns to alpha.

3.3. Biophysics and the Shape of STRCs

As described above, the shape of the STRC predicts the ability of coupled oscillators in the model circuit to synchronize. Similarly, changes in the shape of the STRC accompany changes in synchrony that occur with transitions from one rhythmic state to another. To understand the biophysics of synchrony, therefore, it suffices to explain the mechanisms that determine the shape of the STRC. In the following two subsections, we explain how intrinsic currents and synaptic interactions determine the STRC shape during each rhythmic state and the changes that occur during the transitions between them.

Conclusions from our analysis in the following two subsections can be summarized as follows. In Section 3.3.1, we examine how the underlying biophysics determine the shape of the STRC for parameter values indicated by the three boxed states in Fig. 3a, but over a range of coupling delays. In all three cases, longer delays result in longer intervals between spikes of the inhibitory doublet. For both gamma and beta rhythms (lower boxed states), coupled oscillators synchronize and, correspondingly, the slope of the STRC is between zero and one. This is because the increasing inhibitory doublet interval delays the subsequent firing of the excitatory neuron, resulting in longer periods for longer delays. For the alpha rhythm (upper boxed state), coupled oscillators are asynchronous and the slope of the STRC is negative. This is because hyperpolarization activated inward currents effectively reverse the role of inhibition so that increasing the doublet interval advances the firing of the excitatory neuron under some conditions.

In Section 3.3.2, we examine how the shape of the STRC changes as the underlying biophysics change along the parameter values indicated by the four labeled lines in Fig. 3b. The transition from gamma to alpha (line i) occurs with increasing levels of g_{AHP} when tonic drive is low. Increasing g_{AHP} hyperpolarizes the excitatory neuron, resulting in stronger I_h and I_T inward currents and in an STRC having negative slope as explained above. The transition from alpha to beta (line ii) occurs with increased levels of tonic drive when g_{AHP} is high. Increased tonic drive depolarizes both the excitatory and inhibitory neuron. In the excitatory neuron, depolarization weakens the hyperpolarization-activated inward currents resulting in a PRC having slope between zero and one. In the inhibitory neuron, depolarization enables an intrinsic inhibitory spike to be produced on each cycle, characteristic of beta. The transition from gamma to beta (line iii) occurs with increasing levels of g_{AHP} when tonic drive is high. Increasing g_{AHP} slows the firing rate of the excitatory neuron. This again enables the inhibitory neuron to generate the intrinsic spike characteristic of beta. Finally, when tonic drive is high, gamma rhythms become asynchronous either with increasing delays or with decreasing levels of g_{AHP} (line iv). Decreasing levels of g_{AHP} increases the firing rate of excitatory neurons. If the excitatory neurons firing rate is sufficiently high, or the coupling delay is sufficiently long, imposed input arrives after the end of the excitatory neuron's cycle, and the slope of the STRC no longer determines the synchronization properties of the system.

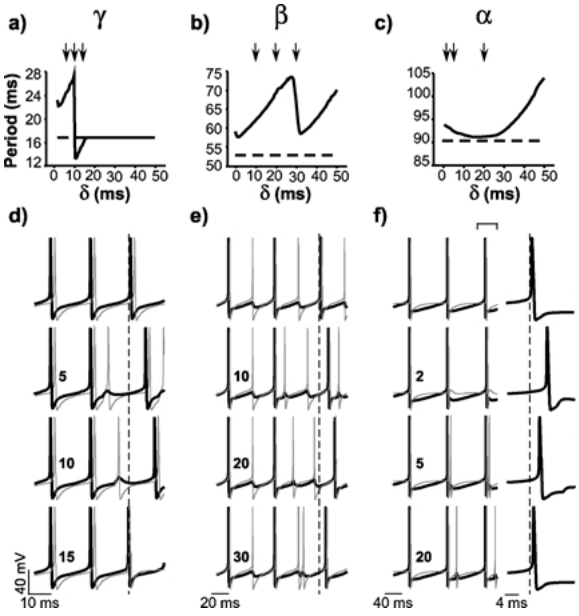

Figure 4. Intrinsic and synaptic properties determine the shape of STRCs. Panels (a)–(c) present STRCs generated from a single cortical oscillator using parameter values for drive and g_{AHP} as indicated by the three boxed values in Fig. 3a; these are the same as Fig. 2e–g. Dashed lines indicate the intrinsic period of the excitatory neuron. Small arrows indicate delays examined in detail in the following panels. Panels (d)–(f) present voltage traces from the excitatory (dark trace) and inhibitory (light trace) neuron of the oscillator while in the same states. Upper traces show the firing patterns of the neurons when the oscillator is unperturbed. Lower traces show the firing patterns of the neurons when an excitatory input is imposed with delay indicated by the small numbers; the delays correspond to the small arrows in panels (a)–(c). Dashed vertical lines are aligned to the third spike of the unperturbed oscillator to emphasize the effect on spike timing of imposed input. The final column in panel (f) presents an expanded view of the third excitatory spike as indicated by the bracket. Note that different time scales are used in each panel.

3.3.1. The Biophysics of Long-Distance Synchrony. We begin by examining more closely the process by which STRCs are constructed. Figure 4a–c present STRCs obtained from a single cortical oscillator using the parameter values indicated by the three boxes in Fig. 3a; these are the same as in Fig. 2e–g. Figure 4d–f present voltage traces from the excitatory (thick black lines) and inhibitory neuron (thin gray lines) of the oscillator from which the STRCs in Fig. 4a–c are constructed. Each trace presents data from two cycles for each rhythm. The upper traces show the firing patterns of the neurons when the oscillator is unperturbed; the duration of the unperturbed firing periods are indicated by the horizontal dashed lines in Fig. 4a–c. Note that the inhibitory neuron exhibits evoked spike singlets rather than doublets during each firing period because it is receiving input only from the excitatory neuron in its local circuit. The lower traces show the firing patterns of the neurons when an excitatory synaptic input is imposed at different delays (δ) after the start of the second cycle; the first cycle is unperturbed and is included for purposes of comparison. The delays are indicated by the numbers in Fig. 4d–f and by the arrows in Fig. 4a–c.

Imposed input results in an additional evoked spike from the inhibitory neuron during the second cycle. In the excitatory neuron, imposed input results in excitation followed by inhibition (due to the imposed inhibitory spike) and also changes the duration of the second cycle. The STRCs in Fig. 4a–c present the duration of the second cycle as a function of the arrival times of the imposed inputs. The dashed vertical lines in Fig. 4d–f are aligned to the end of the second period of the unperturbed oscillator to emphasize the effect on spike timing of imposed inputs. Note that different time scales are used for each rhythmic state. The last column of Fig. 4f presents an expanded view of the final spike during alpha as indicated by the square brackets.

We now examine more closely the relationship between the slope of the STRC at different delays and the intrinsic and synaptic properties of the oscillator during each rhythm. During gamma rhythms (Fig. 4a and d), the STRC has a slope that is positive but less than one for most delays up to the period of the excitatory neuron. As shown in Fig. 4d, inhibition evoked by the imposed inhibitory spike delays the firing of the excitatory neuron ($\delta = 5$). Moreover, the firing delay increases with the delay of imposed input (compare $\delta = 5$ with $\delta = 10$), resulting in a STRC having positive slope. The sharp jump in the STRC in Fig. 4a ($\delta = 15$) marks the point at which the delay of imposed input (δ) is close to the unperturbed firing period of the excitatory neuron. That is, as shown in the last trace of Fig. 4d, if imposed input arrives just before the excitatory neuron fires, the excitatory spike is slightly advanced. If the delay is more than 18 ms, then imposed input arrives after the end of the period of the excitatory neuron.

During beta rhythms (Fig. 4b and e), the STRC has a slope that is positive but less than one over a wider range of input delays than during gamma. Beta rhythms are characterized by an extra intrinsic inhibitory spike during each cycle. As shown in Fig. 4e, the imposed inhibitory spike resets the period of the inhibitory neuron so that the intrinsic spike is delayed ($\delta = 10$). In turn, this delays the firing of the excitatory neuron. Moreover, as with gamma, the firing delay increases with the delay of imposed input (compare $\delta = 10$ with $\delta = 20$), resulting in a STRC having positive slope. If the intrinsic spike is delayed beyond the period of the excitatory neuron (cf. Fig. 6d below) or if the imposed spike does not occur until after the intrinsic spike ($\delta = 30$), then inhibition from the imposed spike delays the firing of the excitatory neuron directly. The relatively sharp jump on the STRC in Fig. 4b ($\delta = 30$) marks the length of the delay at which this occurs.

During alpha rhythms (Fig. 4c and f), the STRC has a slope that is negative for short delays and positive for long delays. Alpha rhythms are characterized by the activation of hyperpolarization activated inward currents. This makes the relationship between the slope of the STRC and the underlying biophysics more subtle than for the cases of gamma and beta rhythms. As shown in Fig. 4f, if imposed input arrives when the inhibitory neuron is still refractory following an evoked spike ($\delta = 2$), then the imposed inhibitory spike does not occur and only excitation is evoked in the excitatory neuron. The resulting depolarization partially deactivates I_h and inactivates the I_T (to be discussed further with Fig. 5 below), resulting in weaker inward currents so that the firing of the excitatory neuron is delayed. If imposed input arrives after the end of the refractory period of the inhibitory neuron ($\delta = 5$), then the imposed inhibitory spike does occur so that excitation followed by inhibition is evoked in the excitatory neuron as before. Inhibition evoked by the imposed spike results in stronger inward currents so that the firing of the excitatory neuron is relatively advanced. Note that the inward currents reverse the role of excitation and inhibition in spike timing; excitation delays firing, inhibition advances firing (see also Jones et al., 2000).

In contrast to the cases of both gamma and beta rhythms, the firing delay of the excitatory neuron during alpha rhythms initially *decreases* with increasing delays of imposed input (compare $\delta = 2$, 5, and 20). This occurs for two reasons. First, as the delay increases from 3 to 5 ms, imposed inputs arrive near the end of the refractory period of the inhibitory neuron but early enough to combine with the remaining influence of the excitatory neuron as discussed above. This causes the inhibitory cell to fire slightly earlier with increasing delays (for details, see Jones et al., 2000). Second, as the delay increases from 5 to 20 ms, the time between the synaptically evoked inhibitory spike and the imposed inhibitory spike increases so that, as shown in Fig. 5a, inhibition evoked by the two spikes becomes less overlapping. As a result, as shown in Fig. 5b, activation of the inward currents increases slightly, and the firing of the excitatory neuron is further advanced.

For long input delays ($\delta > 20$), the firing delay of the excitatory neuron during alpha rhythms increases with increasing delays of imposed input, as with both gamma and beta rhythms. This occurs because the excitatory neuron will fire only after synaptic inhibition has decayed sufficiently, even when the inward currents are active. The inward currents decay more slowly than synaptic inhibition; the time constant of $GABA_A$ is faster than that of either I_h or I_T (Destexhe et al., 1996; also see Fig. 5b). Thus, if imposed input arrives early (e.g., $\delta = 2$ or 5), or the period of the excitatory neuron is long, then synaptic inhibition has sufficient time to decay and the inward currents will advance the firing of the excitatory neuron, as described above. By contrast, if imposed input arrives late ($\delta > 20$), or the period of the excitatory neuron is short (cf. Fig. 6 below), then inhibition will delay directly the firing of the excitatory neuron. In the latter case, the firing delay increases with input delay, as with both gamma and beta, resulting in a STRC having positive slope for long delays.

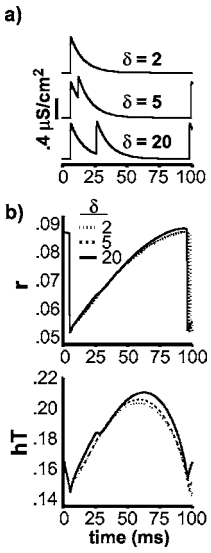

Figure 5. Inward currents reverse the role of inhibition. Panel (a) shows inhibitory synaptic currents evoked in the excitatory neuron of a cortical oscillator when imposed input arrives with a delay of 2, 5, or 20 ms. Longer delays result in inhibition that is less overlapping. Panel (b) shows the time course over one cycle of I_h activation (r) and I_T deinactivation (h_T) when imposed input arrives with the same delays as in panel (a).

3.3.2. The Biophysics of Transitions. As described above, the shape of the STRC during each rhythmic state is determined both by intrinsic currents and by synaptic interactions. Intrinsic currents are affected, both directly and indirectly, by changes in neuromodulation that accompany transitions between rhythmic states. In this section, we examine in detail how neuromodulation affects intrinsic currents and transforms the shape of the STRC during the four transitions (i–iv) indicated on Fig. 3b.

When the level of tonic drive is low, transitions between alpha and gamma rhythms occur with changing levels of g_{AHP}. Figure 6a presents a series of STRCs obtained from a single cortical oscillator, as in Fig. 4a–c, using the parameter values indicated by the horizontal line i in Fig. 3b. As g_{AHP} increases, the STRC shifts upward, its slope over short delays becomes negative, and the sharp jump occurs later. These changes can be understood in terms of the effect of g_{AHP} on the intrinsic and firing properties of the excitatory neuron; increasing g_{AHP} hyperpolarizes the excitatory neuron, lengthens its firing period, and thus raises the STRC. Longer firing periods allow time for synaptic inhibition to decay so that the firing of the excitatory neuron can be advanced by inward currents, as described above. Moreover, increased hyperpolarization results in higher levels of inward current. As shown in Fig. 6b, both I_h activation (r) and I_T deinactivation (h_T) increase with g_{AHP}. Taken together, these effects result in the excitatory neuron firing earlier with increasing delays and hence in the STRC having negative slope. The sharp jump marks the point at which the delay of imposed input is close to the firing period of the excitatory neuron as described above for gamma rhythms. Thus, the jump occurs with longer delays as the period increases.

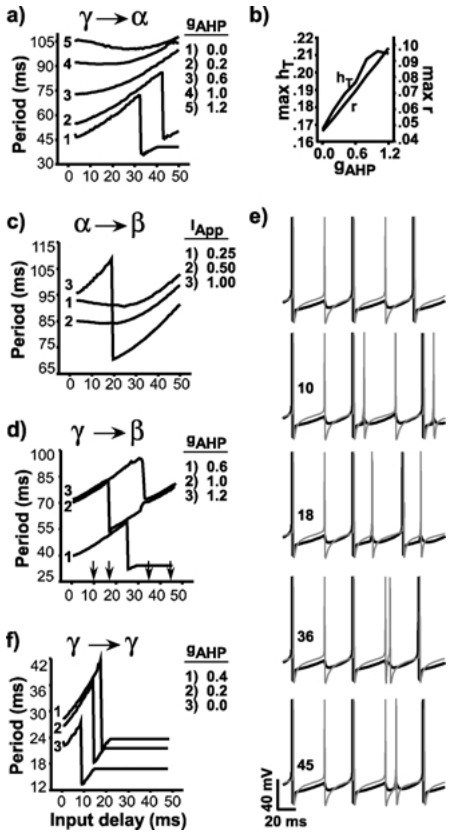

Figure 6. Modulation of intrinsic currents changes the shape of STRCs. Panel (a) presents a series of STRCs generated from a single cortical oscillator using parameter values for drive and g_{AHP} as indicated by line i in Fig. 3b. Panel (b) presents a plot of maximal values of I_h activation (r) and I_T deinactivation (h_T) for the same parameter states as in panel (a). Panels (c), (d), and (f) present series of STRCs generated from the same cortical oscillator as in panel (a) but while in parameter states indicated by line ii, iii, and iv in Fig. 3b, respectively. Panel (e) presents voltage traces from the excitatory (dark trace) and inhibitory (light trace) neuron of the oscillator while in the parameter state indicated by STRC 2 in panel (d). Upper traces show the firing patterns of the neurons when the oscillator is unperturbed. Lower traces show the firing patterns of the neurons when excitatory input is imposed with delay indicated by the small numbers; the delays correspond to the small arrows in panel (d).

When the level of g_{AHP} is high, transitions between alpha and beta occur with changing levels of tonic drive. Figure 6c presents a series of STRCs obtained from the same oscillator as in Fig. 6a, but using the parameter values indicated by the vertical line ii in Fig. 3b. As tonic drive increases, the STRC initially lowers, and its slope becomes gradually more positive (compare STRC 1 and STRC 2). The STRC then shifts drastically upward for short delays and exhibits a sharp jump (STRC 3, $\delta = 20$). To explain this, we note that increasing tonic drive depolarizes the excitatory neuron, resulting in a shorter firing period and thus lowering the STRC. Moreover, depolarization also weakens the inward currents so that the slope of the STRC becomes more positive. Finally, if tonic drive is sufficiently large, the inhibitory neuron will generate an intrinsic spike on each cycle; the firing rate of the excitatory neuron changes more slowly due to high levels of g_{AHP}. Inhibition from the intrinsic spike lengthens the period of the excitatory neuron and shifts the STRC upward. The sharp jump marks the point at which the imposed spike delays the intrinsic spike beyond the period of the excitatory neuron, as described above for beta rhythms.

When the level of tonic drive is high, transitions between gamma and beta occur with changing levels of g_{AHP}. Figure 6d presents a series of STRCs obtained from the same oscillator as in Fig. 6a and c, but using the parameter values indicated by the horizontal line segment iii on Fig. 3b. As g_{AHP} increases, the STRC shifts drastically upward and the jump first occurs earlier and then occurs later. This happens because increasing g_{AHP} hyperpolarizes the excitatory neuron and slows its firing rate while the rate of the inhibitory neuron remains the same. When g_{AHP} is sufficiently large, the inhibitory neuron generates an intrinsic spike during each of its cycles. Inhibition from the intrinsic spike lengthens the period of the excitatory neuron and shifts the STRC upward.

When g_{AHP} is low (STRC 1, Fig. 6d), the sharp jump marks the point at which the imposed delay is close to the firing period of the excitatory neuron, as described above for gamma. When g_{AHP} is high, the sharp jump marks either the point at which the imposed spike delays the intrinsic inhibitory spike beyond the end of the period of the excitatory neuron (STRC 2) or the point at which the imposed spike occurs after the intrinsic spike (STRC 3). Both effects can be seen in Fig. 6e, which presents voltage traces from one of the oscillators, similar to Fig. 4e and f, while in the same state used to generate STRC 2 on Fig. 6d. When $\delta = 18$, the intrinsic spike is delayed beyond the period of the excitatory neuron. When $\delta = 36$, the imposed spike occurs after the intrinsic spike; note the small bump on STRC 2 corresponding to the sharp jump on STRC 3. Note also that the STRCs have negative slope for delays near the sharp jumps. These correspond to the narrow band of asynchronous parameter states between the regions of gamma and beta rhythms on the matrices of Fig. 3.

When the level of tonic drive is high, high frequency gamma rhythms are synchronous over short distances ($\delta = 5$, Fig. 3a) but can be asynchronous over long distances ($\delta = 15$ ms, Fig. 3b). An analogous transition occurs with changing levels of g_{AHP}. Both transitions can be understood in terms of the timing of imposed input relative to the intrinsic firing period of the excitatory neuron. Figure 6f presents a series of STRCs obtained from the same oscillator as above, but using the parameter values indicated by horizontal line segment iv on Fig. 3b. As g_{AHP} decreases, the sharp jump on the STRC occurs at shorter delays, reflecting the shorter firing period of the excitatory neuron, as described above for gamma. For short delays, the STRC has slope between zero and one, and coupled oscillators synchronize. For long delays, imposed input arrives after the end of the firing period of the excitatory neuron.

3.4. Transitions in Layered or Heterogeneous Networks

The analysis presented above is valid only for identical pairs of coupled oscillators. Numerical results suggest, however, that activity in either heterogeneous or layered networks are characterized by similar transitions in both frequency and synchrony.

To examine activity in heterogeneous networks, we constructed a network of four cortical oscillators segregated into two pairs; oscillators within a pair are synaptically connected to each other with no conduction delay (i.e., locally) and to the two oscillators of the other pair with conduction delay δ (i.e., spatially separated). Neurons within a local circuit are connected in all-to-all fashion and include inhibitory connections between local oscillators. Heterogeneity was introduced either by varying independently the synaptic connection strengths and/or applied current to each neuron by $\pm 10\%$ of their normal values, or by adding uniformly distributed random noise ranging from $\pm .2$ μA/cm^2 to the applied current. Results were similar to those presented above for the network of only two cortical oscillators. When the level of tonic drive is high and g_{AHP} is low, the four oscillator network exhibited synchronous gamma rhythms; when g_{AHP} is high, it exhibited synchronous beta rhythms. When the level of tonic drive is low and g_{AHP} is low, the four oscillator networks exhibited synchronous gamma rhythms at low frequency; when g_{AHP} is high, it exhibited asynchronous alpha rhythms. Transitions between rhythmic states were similar to those reported above but were characterized by more complex activity patterns (e.g., clustering). In general, frequency, synchrony, and transitions were all robust in the presence of heterogeneities (however, see discussion).

To examine activity in a layered network, we again constructed a network of four cortical oscillators, but removed the h- and T-currents from the excitatory neuron of one oscillator from each pair. Oscillators lacking h- and T-currents represent layer II/III neurons while oscillators containing h- and T-currents represent layer V neurons. Results were similar to those described above for the heterogeneous network. However, in the layered network, only the oscillators that contained h- and T-currents were intrinsically active during alpha rhythms.

4. Discussion

Motivated by previous experimental and theoretical studies, we have examined a model oscillatory cortical circuit to explore possible biophysical mechanisms underlying behavioral state-dependent transitions in frequency and synchrony of rhythmic cortical activity. Changes in arousal are represented according to known effects of acetylcholine (ACh) on the biophysical properties of individual neurons. Using the model, we demonstrate that such effects are sufficient to induce a transition in rhythmic activity between alpha, beta, and gamma rhythms in a manner consistent with changing behavioral states. Transitions in rhythm are accompanied by corresponding transitions in synchrony over cortical distance in a manner consistent with experimental data. We explain the relationship between these network behaviors and the underlying biophysics using spike time response curves (STRCs). STRCs describe the response of single cortical oscillators to externally imposed input, have shapes that depend on the underlying biophysics, and predict whether or not coupled cortical oscillators will synchronize. Conditions for the accurate use of STRC's are spelled out in the Methods section, as is the supporting evidence for the validity of those conditions in the present case.

Previous studies have used similar analyses to explain individually the biophysics of gamma (Ermentrout and Kopell, 1998), beta (Kopell et al., 2000), and alpha rhythms (Jones et al., 2000). In the current model, we include the conductances needed for all three rhythms to show that a single cortical circuit can support rhythmic activity of each type and to provide a coherent explanation for how neuronal dynamics

can be transformed by neuromodulation. We note also that the mechanism for alpha rhythms proposed here and in Jones et al. (2000) depends only on the presence, but not the details, of some type of hyperpolarization activated inward current that can reverse the role of inhibitory doublets and that has an activation time scale comparable to alpha.

In this and previous studies, STRC analysis contributes beyond simply summarizing the results of the full model in two important ways. First, it provides a means of understanding the networks behavior by examining a relatively small and simple subset of simulations, i.e. the time delay of a single spike. Second, it provides a simple link between the intrinsic and synaptic properties of the network and the network's global behavior. That is, to understand the behavior of the full network, we need only understand how the intrinsic and synaptic properties contribute to the shape of the STRC. In more practical terms, the relationship between STRC shape and synchrony is easily established by means of the analysis reviewed in Methods. The relationship between the STRC and the underlying biophysics can be understood via simulations, as described in Section 3.3, that illuminate how the kinetics of different currents change the shape of the STRC (also see Jones et al., 2000; Kopell et al., 2000; Ermentrout and Kopell, 1998). Note that the latter relationship can also be obtained experimentally. Current studies by ourselves and others are investigating experimentally determined STRCs and their ability to predict synchrony in oscillating pairs of real neurons in neocortex and hippocampus (John White, Theoden Netoff, personal communication).

Our analysis of synchrony over cortical distance can not be extended directly to the study of synchrony in strictly local networks. In particular, a pair of cortical oscillators coupled with a delay $\delta = 0$ is *not* the same as a local circuit with four neurons. This is true for two reasons. First, as discussed in Methods, the strengths of distant excitatory synapses are weaker than those of local synapses. Second, and more importantly, only excitatory neurons form distant synapses in the present model. Thus, the circuit corresponding to $\delta = 0$ has only half the inhibitory synapses of a proper local circuit. Understanding synchrony in large local circuits is likely to require analytic strategies different than those used here.

Our results suggest that, under conditions that lead to alpha rhythms, coupled oscillators are asynchronous across short delays but can be synchronous over longer delays. Moreover, while not examined systematically, we observed that pairs of oscillators tend to phase-lock during alpha (see Fig. 2j and also Jones et al., 2000). Both results are consistent with experimental data demonstrating a phase shift and wave-like activity patterns over cortical space during alpha rhythms in behaving animals (von Stein et al., 2000; Roelfsema et al., 1997). Taken together, these observations suggest that further analysis of the mechanisms underlying alpha rhythms will likely reveal more complex and interesting spatiotemporal activity patterns than those examined here.

Synchrony (or asynchrony) in all of the parameter states we examined was robust to modest changes in both heterogeneity and network size (cf. Section 3.3.2). Surprisingly, this was true not only for parameter states corresponding to experimentally observable rhythms (i.e., alpha, beta, and fast gamma rhythms; the three boxed states in Fig. 3a), but also for parameter states corresponding to synchronous slow gamma rhythms that to our knowledge are not observed experimentally (upper left region of the matrix in Fig. 3a). However, in networks larger than those examined here (i.e., hundreds of neurons), simulations suggest that slow gamma rhythms are more fragile to noisy applied currents than are fast gamma rhythms (Christoph Borgers, David McMillen and Nancy Kopell, personal communication).

A number of alternative mechanisms might explain both the generation of rhythmic brain activity and the transitions between them. For instance, both alpha and gamma rhythms have been observed in the intracellular responses of neurons from thalamus and cortex (Steriade et al., 1993; Silva et al., 1991), suggesting a possible role for thalamocortical projections (see also Nicolelis and Fanselow, 2002). In addition, chattering neurons in cortical layer II/III (Gray and McCormick, 1996) and bursting neurons in layer V (Silva et al., 1991) exhibit rhythmic activity in the gamma and alpha frequency ranges, respectively, suggesting that they might serve as rhythmic pacemakers. Moreover, neuromodulators other than ACh (e.g., serotonin) are also involved in state-dependent changes in activity and are known to have slightly different effects on cortical circuitry (Deteri et al., 1999; Hasselmo, 1995; McCormick, 1992). Despite these limitations, however, our methods and many of our results can be readily adapted to understand the mechanisms underlying rhythm, synchrony, and transitions in oscillating cortical circuits under a broad range of conditions.

Acknowledgments

We thank Andrea Bibbig for pointing out additional literature in support of our alpha rhythm model. D.J. Pinto was supported by NSF G.I.G. grant DMS-9631755, NIH NS25983, and DA 12500. S.R. Jones was supported by a grant from the NSF. T. Kaper was supported by NSF grant 0072596. N. Kopell was supported by NIH grant R01 NS46058.

References

Acker CD, White JA, Kopell N (2002) Synchronization of strongly coupled excitatory neurons: Relating network behavior to biophysics. J. Comput. Neurosci. (submitted).

Bibbig A, Faulkner HJ, Whittington MA, Traub RD (2001) Self-organized synaptic plasticity contributes to the shaping of gamma and beta oscillations *in vitro*. J. Neurosci. 21(22): 9053–9067.

Buzsaki G, Bickford RG, Ponomareff G, Thal LJ, Mandel RJ, Gage FH (1988) Nucleus basalis and thalamic control of neocortical activity in the freely moving rat. J. Neurosci. 8(11): 4007–4026.

Cape EG, Jones BE (1998) Differential modulation of high-frequency γ-electroencephalogram activity and sleep-wake state by noradrenaline and serotonin microinjections into the region of cholinergic basalis neurons. J. Neurosci. 18(7): 2653–2666.

Cape EG, Jones BE (2000) Effects of glutamate agonist versus procaine microinjections into the basal forebrain cholinergic cell area upon gamma and theta EEG activity and sleep-wake state. Eur. J. Neurosci. 12: 2166–2184.

Castro-Alamancos MA, Connors BW (1996a) Short-term plasticity of a thalamocortical pathway dynamically modulated by behavioral state. Science 272: 274–277.

Castro-Alamancos MA, Connors BW (1996b) Cellular mechanisms of the augmenting response: Short-term plasticity in a thalamocortical pathway. J. Neurosci. 16(23): 7742–7756.

Celesia GG, Jasper HH (1966) Acetylcholine released from cerebral cortex in relation to state of activation. Neurologist 16: 1053–1064.

Chow CC, White JA, Ritt J, Kopell N (1998) Frequency control in synchronized networks of inhibitory neurons. J. Comput. Neurosci. 5: 407–420.

Connors BW, Amitai Y (1997) Making waves in the neocortex. Neuron 18: 347–349.

da Silva LF (1991) Neural mechanisms underlying brain waves: From neural membranes to networks. Electroenceph. Clin. Neurophysiol. 79: 81–93.

De La Pena E, Geijo-Barrientos E (1996) Laminar localization, morphlogy, and physiological properties of pyramidal neurons that have low-threshold calcium current in the guinea-pig medial frontal cortex. J. Neurosci. 16: 5301–5311.

Destexhe A, Babloyantz A, Sejnowski TJ (1993) Ionic mechanisms for intrinsic slow oscillations in thalamic relay neurons. Biophys. J. 65: 1538–1552.

Destexhe A, Bal T, McCormick D, Sejnowski TJ (1996) Ionic mechanisms underlying synchronized oscillations and propagating waves in a model of ferret thalamic slices. J. Neurophysiol. 76: 2049–2070.

Destexhe A, Mainen ZF, Sejnowski TJ (1998) Kinetic models of synaptic transmission. In: C. Koch, I. Segev, eds. Methods in Neuronal Modeling, 2nd ed. MIT Press, Cambridge.

Detari L, Rasmusson DD, Semba K (1999) The role of basal forebrain neurons in tonic and phasic activation of the cerebral cortex. Prog. Neurobiol. 58: 249–277.

Devaney RL (1992) A First Course in Chaotic Dynamical Systems: Theory and Experiment. Addison-Wesley, Reading, MA.

Dringenberg HC, Vanderwolf CH (1997) Neocortical activation: Modulation by multiple pathways acting on central cholinergic and serotonergic systems. Exp. Brain Res. 116: 160–174.

Ermentrout GB, Kopell N (1998) Fine structure of neural spiking and synchronization in the presence of conduction delays. PNAS 95: 1259–1264.

Fanselow EE, Nicolelis MAL (1999) Behavioral modulation of tactile responses in the rat somatosensory system. J. Neurosci. 19: 7603–7616.

Farmer SF (1998) Rhythmicity, synchronization and binding in human and primate motor systems. J. Physiol. 509(1): 3–14.

Fuchs EC, Doheny H, Faulkner H, Caputi A, Traub RD, Bibbig A, Kopell N, Whittington MA, Monyer H (2000) Genetically altered AMPA-type glutamate receptor kinetics in interneurons disrupt long-range synchrony of gamma oscillation. PNAS 96(6): 3571–3576.

Gray CM, McCormick DA (1996) Chattering cells: Superficial pyramidal neurons contributing to the generation of synchronous oscillations in the visual cortex. Science 274(5284): 109–113.

Haenschel C, Baldeweg T, Croft RJ, Whittington M, Gruzelier J (2000) Gamma and beta frequency oscillations in response to novel auditory stimuli: A comparison of human electroencephalogram (EEG) data with *in vitro* models. PNAS 97: 7645–7650.

Hasselmo ME (1995) Neuromodulation and cortical function: Modeling the physiological basis of behavior. Behav. Brain Res. 67: 1–27.

Jones SR, Pinto DJ, Kaper TJ, Kopell N (2000) Alpha-frequency rhythms desynchronize over long cortical distances: A modeling study. J. Comput. Neurosci. 9: 271–291.

Karbowski J, Kopell N (2000) Multispikes and synchronization in a large neural network with temporal delays. Neural Comp. 12: 1573–1606.

Keil A, Gruber T, Muller MM (2001) Functional correlates of macroscopic high-frequency brain activity in the human visual system. Neurosci. and Biobehavioral Rev. 25: 527–534.

Kisvarday ZF, Kim DS, Eysel UT, Bonhoeffer T (1994) Relationship between lateral inhibitory connections and the topography of the orientation map in cat visual corex. Eur. J. Neurosci. 6(10): 1619–1632.

Kristiansen K, Courtois G (1949) Rhythmic electrical activity from isolated cerebral cortex. EEG Clin. Neurophysiol. 1: 265–272.

Kopell N, Ermentrout GB, Whittington MA, Traub RD (2000) Gamma rhythms and beta rhythms have different synchronization properties. PNAS 97(4): 1867–1872.

Lo Conte G, Casamenti F, Bigi V, Milaneshi E, Pepeu G (1982) Effect of magnocellular forebrain lesions on acetylcholine output from the cerebral cortex, electrocorticogam and behavior. Arch. Ital. Biol. 120: 176–188.

Lund J, Yoshioka T, Levitt J (1993) Comparison of intrinsic connectivity in different areas of macaque monkey cerebral-cortex. Cerebral Cortex 3: 148–162.

Marrufo MV, Vaquero E, Cardoso MJ, Gomez CM (2001) Temporal evolution of α and β bands during visual spatial attention. Cog. Brain Res. 12: 315–320.

McCormick DA (1992) Neurotransmitter actions in the thalamus and cerebral cortex. J. Clin. Neurophysiol. 9(21): 212–223.

Muller MM (2000) Oscillatory cortical activities in the gamma band in the human EEG induced by visual stimuli—representation of the stimulus? Acta Neurobiol. Exp. 60: 49–65.

Nicolelis MAL, Fanselow EE (2002) Thalamocortical optimization of tactile processing according to behavioral state. Nature Neurosci. 5(6): 517–523.

Nunez PL, Wingeier BM, Silberstein RB (2001) Spatial-temporal structures of human alpha rhythms: Theory, microcurrent sources, multiscale measurements, and global binding of local networks. Human Brain Mapping 13(3): 125–164.

Pantev C (1995) Evoked and induced gamma band activity of the human cortex. Brain Topog. 7: 321–330.

Pare D, Lang EJ (1998) Calcium electrogenesis in neocortical pyramidal neurons *in vivo*. Eur. J. Neuosci. 10: 3164–3170.

Roelfsema PR, Engel AK, König P, Singer W (1997) Visuomotor integration is associated with zero time-lag synchronization among cortical areas. Nature 385: 157–161.

Sherman SM (2001) Tonic and burst firing: Dual modes of thalamocortical relay. Trends Neurosci. 24(2): 122–126.

Silva LR, Amitai Y, Connors BW (1991) Intrinsic oscillations of neocortex generated by layer 5 pyramidal neurons. Science 251: 432–435.

Steriade M, McCormick DA, Sejnowski TJ (1993) Thalamocortical oscillations in the sleeping and aroused brain. Science 262: 679–685.

Steriade M, Timofeev I, GrenierF, Durmuller N (1998) Role of thalamic and cortical neurons in augmenting responses and self-sustaining activity: Dual intracellular recordings *in vivo*. J Neurosci. 18: 6425–6443.

Tallon-Baudry C, Bertrand O (1999) Oscillatory gamma activity in humans and its role in object representation. Trends Cog. Sci. 3(4): 151–162.

Timofeev I, Grenier F, Bazhenov M, Houweling AR, Sejnowski TJ, Steriade M (2002) Short- and medium-term plasticity associated with augmenting responses in cortical slabs and spindles in intact cortex of cats *in vivo*. J. Physiol. 542(2): 583–598.

Traub RD, Jefferys JGR, Whittington MA (1997) Simulation of gamma rhythms in networks of interneurons and pyramidal cells. J. Comput. Neurosci. 4(2): 141–150.

Traub RD, Jefferys JGR, Whittington MA (1999) Fast Oscillations in Cortical Circuits. MIT Press, Cambridge.

Traub RD, Whittington MA, Buhl EH, Jefferys JGR, Faulkner HJ (1999) On the mechanism of the $\gamma \rightarrow \beta$ frequency shift in neuronal oscillations induced in rat hippocampal slices by tetanic stimulation. J. Neurosci. 19(3): 1088–1105.

Traub RD, Whittington MA, Colling SB (1996) Analysis of gamma rhythms in the rat hippocampus *in vitro* and *in vivo*. J. Physiol. London 493(2): 471–484.

von Stein A, Rappelsberger P, Sarnthein J, Petsche H (1999) Synchronization between temporal and parietal cortex during multimodal object processing in man. Cerebral Cortex 9(2): 137–150.

von Stein A, Sarnthein J (2000) Different frequencies for different scales of cortical integration: From local gamma to long range alpha/theta synchronization. Int. J. Psychophysiol. 38(3): 301–313.

Wang XJ, Golomb D, Rinzel J (1995) Emergent spindle oscillations and intermittent burst firing in a thalamic model: Specific neuronal mechanisms. PNAS 92: 5577–5581.

White EL (1989) Cortical Circuits: Synaptic Organization of the Cerebral Cortex. Structure, Function, and Theory. Birkhauser, Boston, MA.

Whittington MA, Traub RD, Faulkner HJ, Stanford IM, Jefferys JGR (1997) Recurrent excitatory postsynaptic potentials induced by synchronized fast cortical oscillations. PNAS 94: 12198–12203.

Whittington MA, Traub RD, Jefferys JGR (1995) Synchronized osillations in interneuron networks driven by metabotropic glutamate-receptor activation. Nature 373(6515): 612–615.

Whittington MA, Traub RD, Kopell N, Ermentrout GB, Buhl EH (2000) Inhibition-based rhythms: Experimental and mathematical observations on network dynamics. Int. J. Psychophysiol. 38: 315–336.

Winfree AT (1980) The Geometry of Biological Time. Springer, New York.